International Journal of Solids and Structures 49 (2012) 2450–2459

Contents lists available at SciVerse ScienceDirect

International Journal of Solids and Structures

journal homepage: www.elsevier.com/locate/ijsolstr

FE analysis of the in-plane mechanical properties of a novel Voronoi-type lattice with positive and negative Poisson's ratio configurations

Mustapha Bouakba [a,b], Abderrezak Bezazi [b], Fabrizio Scarpa [c,*]

[a] Université Kasdi Merbah Ouargla, Route de Ghardaia 30000, Algeria
[b] Laboratoire de Mécanique & Structures (LMS), BP. 401, Université 08 Mai 1945, Guelma 24000, Algeria
[c] Advanced Composites Centre for Innovation and Science (ACCIS), University of Bristol, BS8 1TR Bristol, UK

ARTICLE INFO

Article history:
Received 16 March 2012
Received in revised form 4 May 2012
Available online 22 May 2012

Keywords:
Lattice structures
Elastic behaviour
Simulation
Finite element analysis

ABSTRACT

This work presents a novel formulation for a Voronoi-type cellular material with in-plane anisotropic behaviour, showing global positive and negative Poisson's ratio effects under uniaxial tensile loading. The effects of the cell geometry and relative density over the global stiffness, equivalent in-plane Poisson's ratios and shear modulus of the Voronoi-type structure are evaluated with a parametric analysis. Empirical formulas are identified to reproduce the mechanical trends of the equivalent homogeneous orthotropic material representing the Voronoi-type structure and its geometry parameters.

1. Introduction

The mechanical and transport properties of cellular solids have been traditionally modeled using periodic unit cells representative volumes. Examples of these unit cell topologies are the hexagonal prismatic and quadrilateral centrosymmetric ones (Gibson and Ashby, 1997), Kelvin lattices (Choi and Lakes, 1995; Zhu et al., 1997; Warren and Kraynik, 1997; Mills, 2005; Gong et al., 2005; Weaire, 2008). The level of disorder associated to the shape and orientation of cells belonging to real open cell foams has been described numerically by making use of Voronoi diagrams (Kraynik et al., 2003). Voronoi tessellations create one-to-one optimal (i.e., minimum distance) correspondence between a point in the space and polytopes (a geometric entity delimited by segments in 2D) to guarantee the creation of six-sided polygons (Lucarini, 2008). Voronoi diagrams have been extensively used to simulate the mechanical properties of open cell foam structures (Silva et al., 1995; Zhu et al., 2001, 2006). The classical Voronoi tessellation (Fig. 1a) generates models related to open cell foams which show a global isotropic mechanical response under linear elastic regime (Silva et al., 1995; Zhu et al., 2001). However, cellular structures (like the balsa wood example in Fig. 1b) may show a specific directionality in terms of average orientation and shape geometry of their cells, therefore providing a global anisotropic mechanical behaviour against a general Cartesian coordinates system. Moreover, polymeric open cell foams (produced in laboratory for replication or pyrolysis applications (Oliveira et al., 2006) do tend to show a general mechanical anisotropic behaviour due to the specific rising direction of the foam during manufacturing. The existence of anisotropic lattices with topologies inspired to disordered or Voronoi-type configurations can be nowadays reproduced using rapid prototyping or other advanced manufacturing processes (Fig. 1c), making possible the study and evaluation of cellular configurations with potentially unusual deformation mechanisms (Schwerdtfeger et al., 2011).

This work describes a mathematical formulation for a Voronoi-like cellular structure with anisotropic mechanical characteristics, different from centroidal Voronoi tessellations (Qiang et al., 1999). The Voronoi diagram proposed in this work consists in using the centroid of the Delaunay triangle as one of the vertex of the new unit cell. Once all vertex are identified, the closing polygon constitutes the new type of Voronoi diagram. This new Voronoi assembly can assume convex or re-entrant cells oriented along two axis defined by a pair of cosine directors. Re-entrant cells are typical of the "butterfly" honeycomb configurations and foams, leading to negative Poisson's ratio (auxetic) behaviour (Gibson and Ashby, 1982; Almgren, 1985; Lakes, 1987; Masters and Evans, 1996; Scarpa et al., 2000, 2003; Grima et al., 2006; Bezazi and Scarpa, 2007, 2009; McDonald et al., 2009). The honeycomb assemblies are translated into a 2D finite element mesh, where the ribs are modeled using Timoshenko beam elements. Uniaxial tensile loading is applied along two orthogonal directions simulating a global Cartesian coordinate system, and the in-plane mechanical properties (Young's moduli along the two directions, and Poisson's ratios)

* Corresponding author.
E-mail addresses: mustapha.bouakba@gmail.com (M. Bouakba), ar_bezazi@yahoo.com (A. Bezazi), f.scarpa@bristol.ac.uk (F. Scarpa).

0020-7683/$ - see front matter Crown Copyright © 2012 Published by Elsevier Ltd. All rights reserved.
http://dx.doi.org/10.1016/j.ijsolstr.2012.05.007

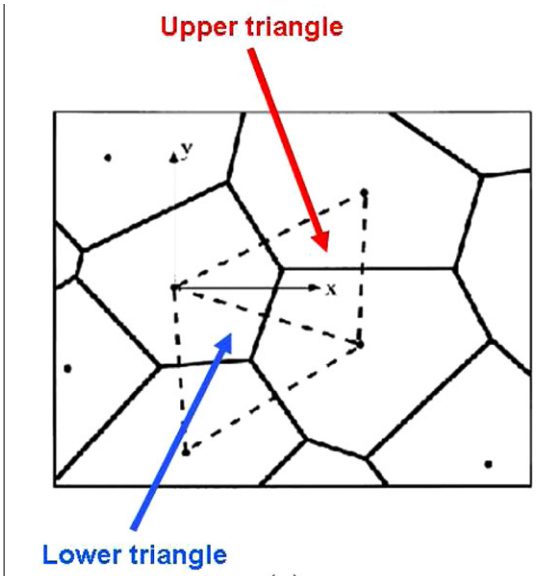

(a)

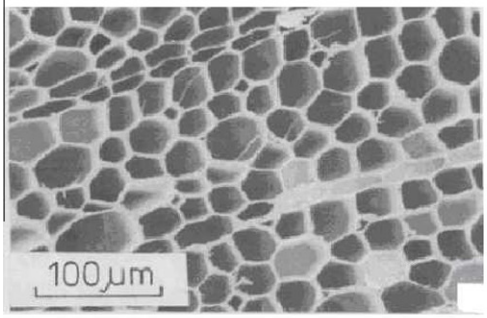

(b)

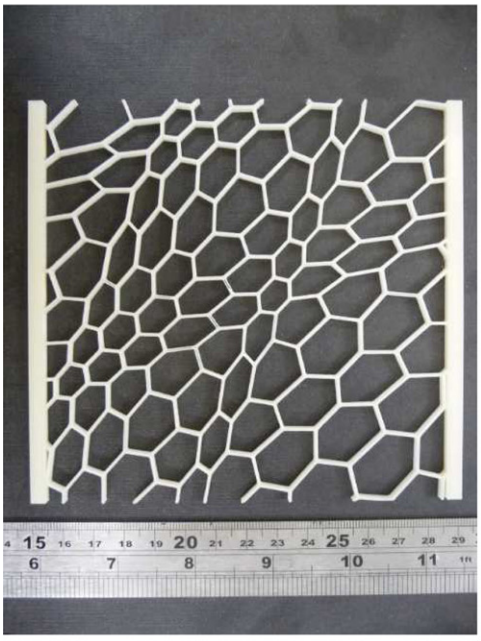

(c)

Fig. 1. (a) Layout of a classical Voronoi honeycomb. (b) Cellular structure of balsa wood (From (Gibson and Ashby, 1997)). (c) Anisotropic lattice made with FDM Rapid Prototyping technique.

are derived for an equivalent homogenous 2D material. The new Voronoi-type porous structures described in this work show anisotropic properties, with Poisson's ratios varying between positive and negative values, and in-plane stiffness properties comparable with the ones of classical Voronoi tessellations. The re-entrant configuration does exhibit lower uniaxial in-plane stiffness values compared with classical Voronoi assemblies, while maintaining global negative Poisson's ratio characteristics when loaded along the two global Cartesian orthogonal directions. The cell walls of these novel Voronoi diagrams show also a complex combination of bending and stretching deformation mechanisms, based on the relative position of the ribs in the cellular assembly.

2. Mathematical description of the cellular structure

2.1. Convex layout

The classic Voronoi tessellation is formed by subtracting segments perpendicular to the base of triangles created linking the centroids of each cell (Fig. 1a) (Silva et al., 1995; Gibson and Ashby, 1997; Andrews and Gibson, 2001; Zhu et al., 2006). From an array of randomly located "nucleation points", a Voronoi diagram is generated by constructing the perpendicular bisectors of each pair of adjacent points. The resulting cells are those which would have formed if they nucleated simultaneously from the points and grew at a uniform rate until they intersected the adjacent cells (Silva et al., 1995).

The mathematical model for the novel type of Voronoi-like tessellation proposed in this work is constituted by a random distribution of N points with coordinates (x_i, y_i) placed along main directions that are defined by cosine directors x_l and y_l. Every element of the cellular tessellation (4 neighboring points forming a parallelogram) is divided into two triangles to create a Delaunay tessellation with angles Φ and Ψ defining a global orientation in the space (Fig. 2a). The new Voronoi tessellation is created linking the centres of the two triangles, with the coordinates of each centre of gravity (C.G.) for the single triangles calculated as:

$$x_{\Delta\text{Lower}}(i,j) = \frac{d(i,j) - b(i,j)}{a(i,j) - c(i,j)} \tag{1}$$

$$y_{\Delta\text{Lower}}(i,j) = a(i,j)x_{\Delta low}(i,j) + b(i,j) \tag{2}$$

$$x_{\Delta\text{Upper}}(i,j) = \frac{h(i,j) - f(i,j)}{e(i,j) - g(i,j)} \tag{3}$$

$$y_{\Delta\text{Upper}}(i,j) = e(i,j)x_{\Delta\text{Upper}}(i,j) + h(i,j) \tag{4}$$

Where $x_{\Delta\text{Lower}}(i,j), y_{\Delta\text{Lower}}(i,j)$ and $x_{\Delta\text{Upper}}(i,j), y_{\Delta\text{Upper}}(i,j)$ are the coordinates of the C.G. for the lower and upper triangles in the local (x,y) plane. The elements $a(i,j), b(i,j), c(i,j), d(i,j), e(i,j), f(i,j), g(i,j)$ and $h(i,j)$ are defined as follows:

$$\begin{aligned}
a(i,j) &= \frac{(x_i - x_{i+1})\sin\Phi + \frac{1}{2}(y_{j+1} - y_j)\cos\Psi}{(x_i - x_{i+1})\cos\Phi + \frac{1}{2}(y_{j+1} - y_j)\sin\Psi} \\
b(i,j) &= x_{i+1}\sin\Phi + y_j\cos\Psi - a(i,j)(x_{i+1}\cos\Phi + y_j\sin\Psi) \\
c(i,j) &= \frac{\frac{1}{2}(x_i - x_{i+1})\sin\Phi + (y_j - y_{j+1})\cos\Psi}{\frac{1}{2}(x_i - x_{i+1})\cos\Phi + (y_j - y_{j+1})\sin\Psi} \\
d(i,j) &= x_i\sin\Phi + y_{j+1}\cos\Psi - c(i,j)(x_i\cos\Phi + y_{j+1}\sin\Psi)
\end{aligned} \tag{5}$$

$$\begin{aligned}
e(i,j) &= \frac{\frac{1}{2}(x_i - x_{i+1})\sin\Phi + (y_{j+1} - y_j)\cos\Psi}{\frac{1}{2}(x_i - x_{i+1})\cos\Phi + (y_{j+1} - y_j)\sin\Psi} \\
f(i,j) &= x_{i+1}\sin\Phi + y_j\cos\Psi - e(i,j)(x_{i+1}\cos\Phi + y_j\sin\Psi) \\
g(i,j) &= \frac{(x_i - x_{i+1})\sin\Phi + \frac{1}{2}(y_j - y_{j+1})\cos\Psi}{(x_i - x_{i+1})\cos\Phi + \frac{1}{2}(y_j - y_{j+1})\sin\Psi} \\
h(i,j) &= x_i\sin\Phi + y_{j+1}\cos\Psi - g(i,j)(x_i\cos\Phi + y_{j+1}\sin\Psi)
\end{aligned} \tag{6}$$

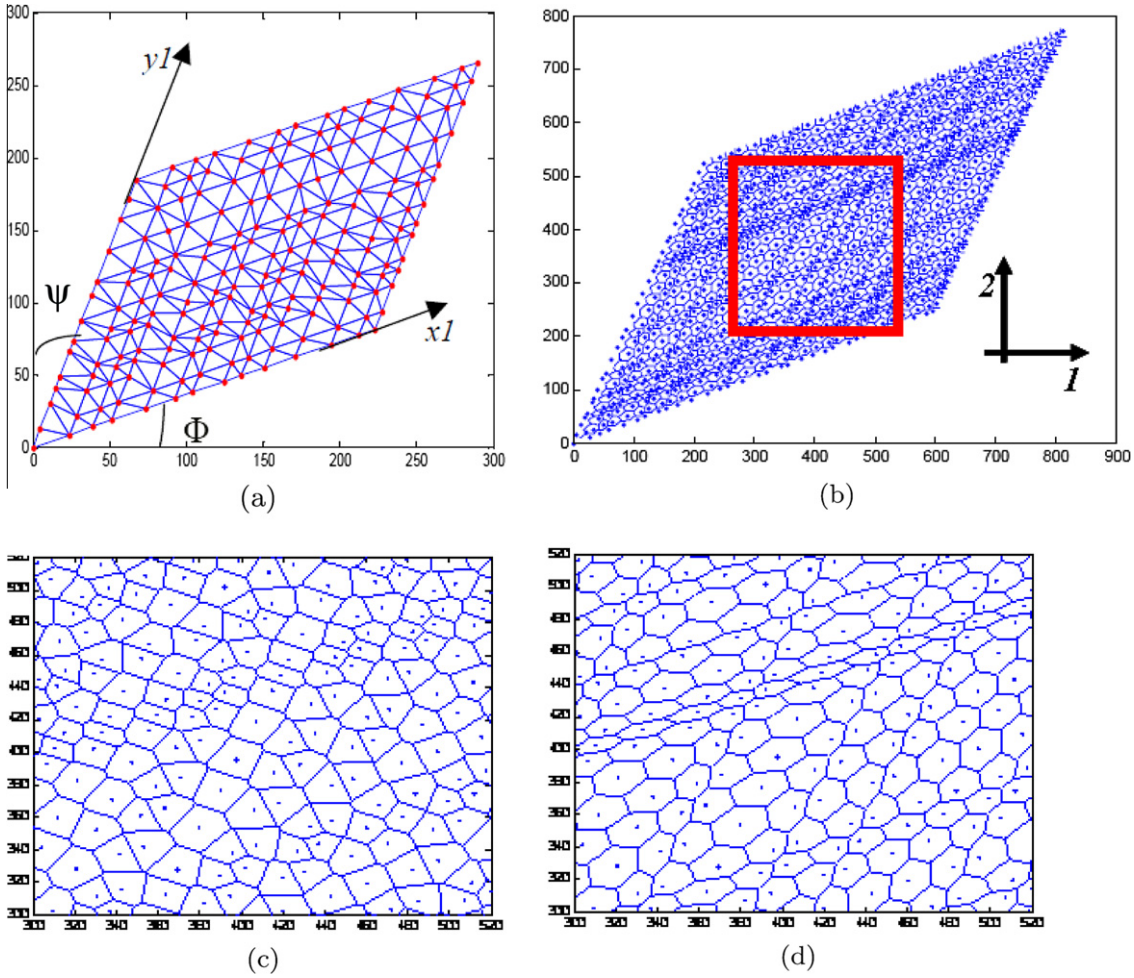

Fig. 2. (a) Delaunay tessellation with cosine directors x_l and y_l forming angles Φ and Ψ with the global Cartesian coordinate system axis $(1,2)$ respectively; (b) A convex honeycomb mesh ($\Phi = \Psi = \pi/8$) for the Finite element simulation is obtained cropping the global tessellation within the red square; (c) Cells layout within a cropped area obtained from the classical Voronoi tessellation; (d) Convex honeycomb layout build with the present approach ($\Phi = \Psi = \pi/8$) and obtained from (b).

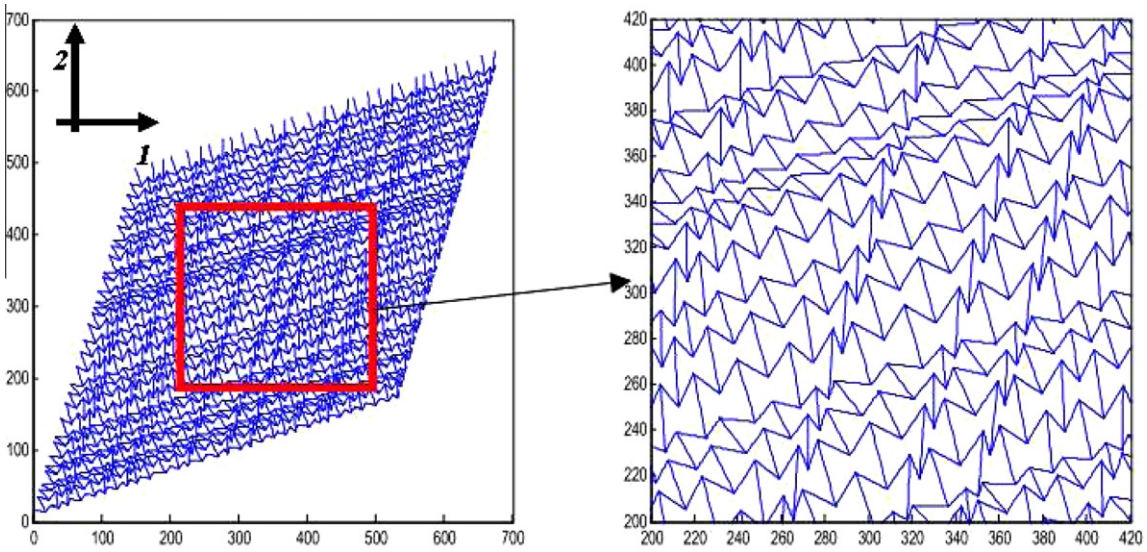

Fig. 3. Proposed Voronoi-type structure with re-entrant sides ($\Phi = \Psi = \pi/8$).

The tessellation is then mapped to any arbitrary plane $(1,2)$ (Fig. 2b). The difference between a classical Voronoi layout and the one proposed for a specific set of angles Φ and Ψ ($\Phi = \Psi = \pi/8$) can be observed in Figs. 2c and 2d.

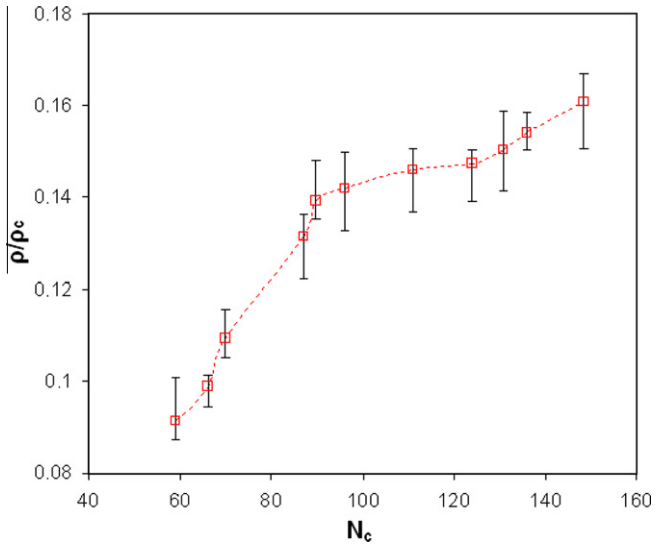

Fig. 4. Variation of the relative density ρ/ρ_c for the convex honeycomb versus the number of cells N_c in the representative volume element.

2.2. Re-entrant (negative Poisson's ratio) layout

It is possible to create a version of the anisotropic Voronoi layout with global re-entrant cells (Fig. 3), which could provide a negative (auxetic) Poisson's ratio behaviour (Gibson and Ashby, 1997;Scarpa et al., 2000). In this case, the first part of Eq. (5) needs to be transformed into:

$$a(i,j) = \frac{(x_i - x_{i+1})\sin\Phi + k(y_{j+1} - y_j)\cos\Psi}{(x_i - x_{i+1})\cos\Phi + k(y_{j+1} - y_j)\sin\Psi} \tag{7}$$

The distance $a(i,j)$ depends in this case by a factor k, which is used to modify the location of the centre of gravity belonging to the lower triangle in the Delaunay tessellation. For $0.5 < k < 1$ the resulting Voronoi-type structure is not auxetic. For $k = 1$ the honeycomb generated shows a general negative Poisson's ratio value, although lower than -0.3. The value of $k = 1.11$ has been observed as being a limiting one, above which the ligaments of the re-entrant cells keep in geometric contact. This limiting value of k has been used through all the simulations described in this work.

2.3. Finite element models

The Voronoi-type honeycomb layouts have been created using a custom-made MATLAB routine, and then exported to the commercial Finite element code ANSYS (ANSYS Manual, 2008). The meshes have been created using two-dimensional Timoshenko beam elements BEAM3 with rectangular cross-section (width of 1 mm), uniform thickness t and 3 degrees of freedom (translational along the global x and y direction, and in-plane rotation along the z-axis). After a convergence test, each rib of the cells was represented by five elements. The uniaxial loading has been represented using the approach from (Silva et al., 1995;Scarpa et al., 2000). When loading along the global 1 direction (Fig. 5), one side was subjected to imposed deformations and zero in-plane rotation, while the opposite one was subjected to a slide boundary condition. The homogenised lateral strains were calculated by averaging the lateral displacements on the transverse sides of the honeycombs, making therefore possible to calculate the in-plane Poisson's ratios using the following equations:

$$\nu_{ij} = -\frac{\epsilon_j}{\epsilon_i} \tag{8}$$

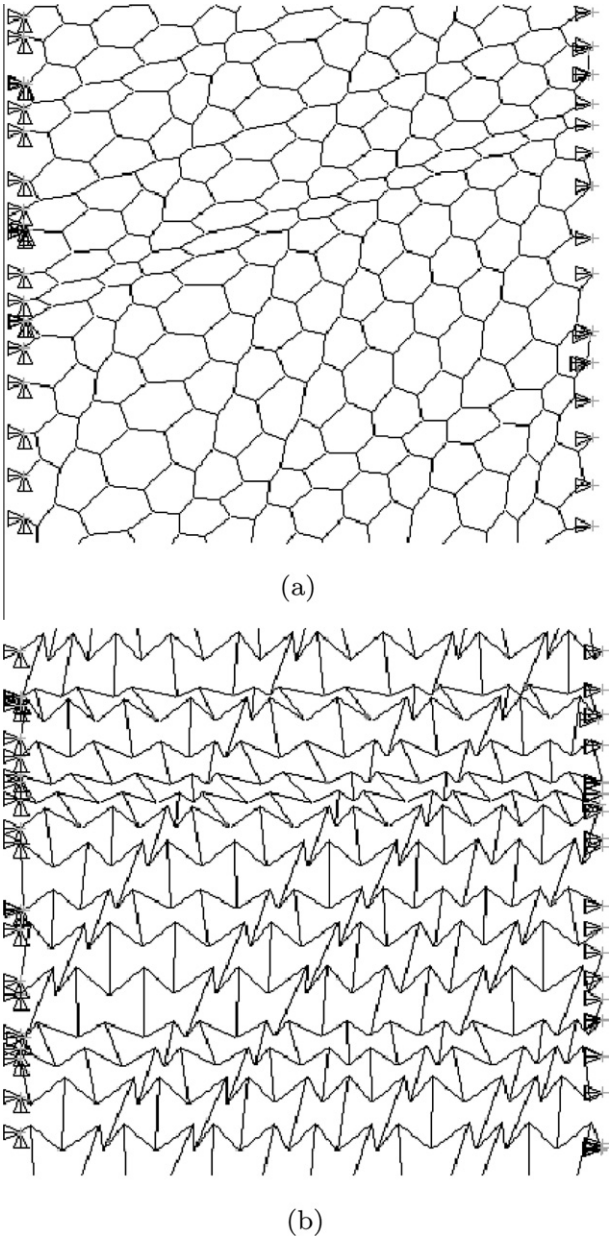

Fig. 5. (a) FE model of the new shape convex honeycomb structure under uniaxial tensile loading; (b) analogous FE representation for the re-entrant (negative Poisson's ratio) version.

Where the subscripts i,j stand for the directions 1 and 2. The axial stresses σ_1 and σ_2 where computed averaging the total sum of the nodal reaction forces on the side subjected to the imposed displacements. The nondimensional in-plane Young's moduli were therefore calculated as:

$$E^*_{i,j} = \frac{E_{i,j}}{E_c} = \frac{\sigma_{i,j}}{\epsilon_{i,j}}\frac{1}{E_c} \tag{9}$$

The shear modulus has been calculated using a biaxial loading (Li et al., 2005), with a compressive strain ε_y and a tensile strain ε_x applied to the top and right sides of the lattice assemblies respectively. The reaction forces F_1 and F_2 have been used to extract the equivalent shear modulus G_{12} as follows:

$$G_{12} = \frac{\frac{F_1}{Y} - \frac{F_2}{X}}{2b(\varepsilon_x - \varepsilon_y)} \tag{10}$$

Where Y and X are the dimensions of the overall lattice along the 2 and 1 global axis respectively (Fig. 2b).

All simulations have been performed considering the material and the structure under linear elastic regime. A series of simulations was carried out freeing the rotations of the ligaments. A free in-plane rotation of the ribs has shown a quasi negligible effect on the uniaxial stiffness values compared to the fixed rotations configurations, with a discrepancy between 0.76% and 0.98% for E_1/E_c and E_2/E_c. The in-plane Poisson's ratios were mostly affected when the in-plane rotations of the ribs were kept free, with percentage errors around 30%. The relative density of the Voronoi-type honeycomb has been calculated considering the following summation (Fazekas et al., 2002):

$$\frac{\rho}{\rho_c} = \sum_i t \frac{l_i}{L_{x1} L_{y1}} \tag{11}$$

Where l_i is the length of each rib composing the honeycomb, and L_{x1}, L_{y1} are the global lengths of the side of the honeycomb assembly. Due to the trigonometric dependence against Φ and Ψ of the locations and lengths of the Voronoi cells in (5–6), the number of cells in the fixed representative volume of Figs. 2b and 3 vary according to the pair of cosine angles used following a linear trend ($N_c = -335.7\Phi + 266$ for $\Phi = \Psi$, with $R^2 = 0.99$), with the overall density of the Voronoi-type honeycomb decreases with increasing magnitudes of the pair of cosine directors. Inspecting Fig. 4, it is possible to identify a quadratic dependence of the relative density (11) versus the number of cells ($\rho/\rho_c = -4.5310^{-6} N_c^2 + 0.0015 N_c + 0.024$, with $R^2 = 0.91$). For a given constant thickness ($t = 1$ mm), the average length l of the ribs does depend on the number of cells and the honeycomb configuration. For the convex honeycomb type, l varies from 11.67 mm for $N_c = 66$ to 9.72 mm for $N_c = 152$. The re-entrant layout shows average values of l varying between 23.7 mm for $N_c = 49$ to 15.7 mm for $N_c = 141$.

All the simulations have been carried out considering aluminum as the reference core material ($E_c = 70$ GPa, $\nu_c = 0.33$). For each configuration of cosine directors and constant rib thickness t five different cellular assemblies have been generated, to obtain average and standard deviation values of the uniaxial mechanical properties.

3. Results and discussions

3.1. Convex configurations

From a topological point of view, the use of different pairs of director angles Φ and Ψ provides a variety of configurations, some examples being shown in Fig. 6, where the distances between the triangulation points are kept constant. Fig. 7a shows the variation of the nondimensional moduli E_1/E_c and E_2/E_c versus the relative density. It is possible to observe power relations of the type

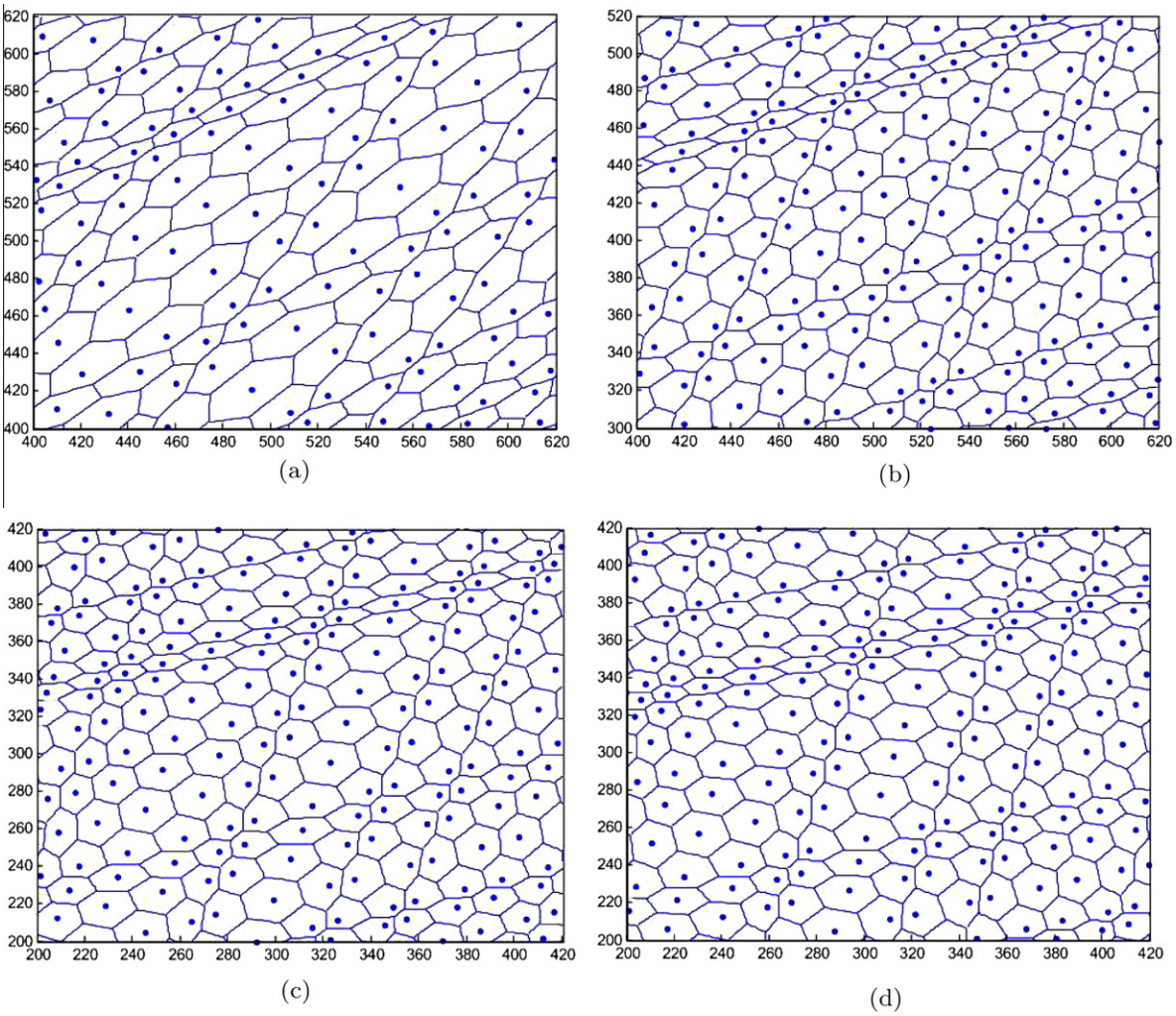

Fig. 6. The influence of the angles Φ and Ψ over the convex honeycomb topology. (a) $\Phi = \Psi = \pi/6$; (b) $\Phi = \Psi = \pi/8$; (c) $\Phi = \Psi = \pi/10$; (d) $\Phi = \Psi = \pi/12$.

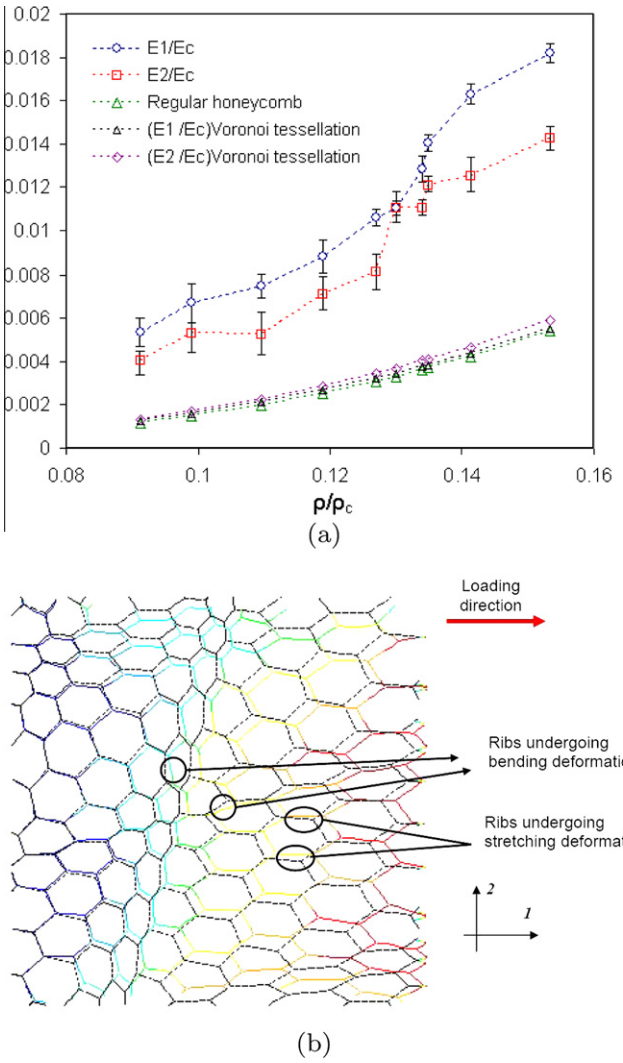

Fig. 7. (a) Evolution of the nondimensional Young's moduli versus the relative density for the convex honeycomb. (b) Deformation mechanisms of the ribs in a convex panel with $\Phi = \Psi = \pi/12$ when subjected to uniaxial loading along the direction 1.

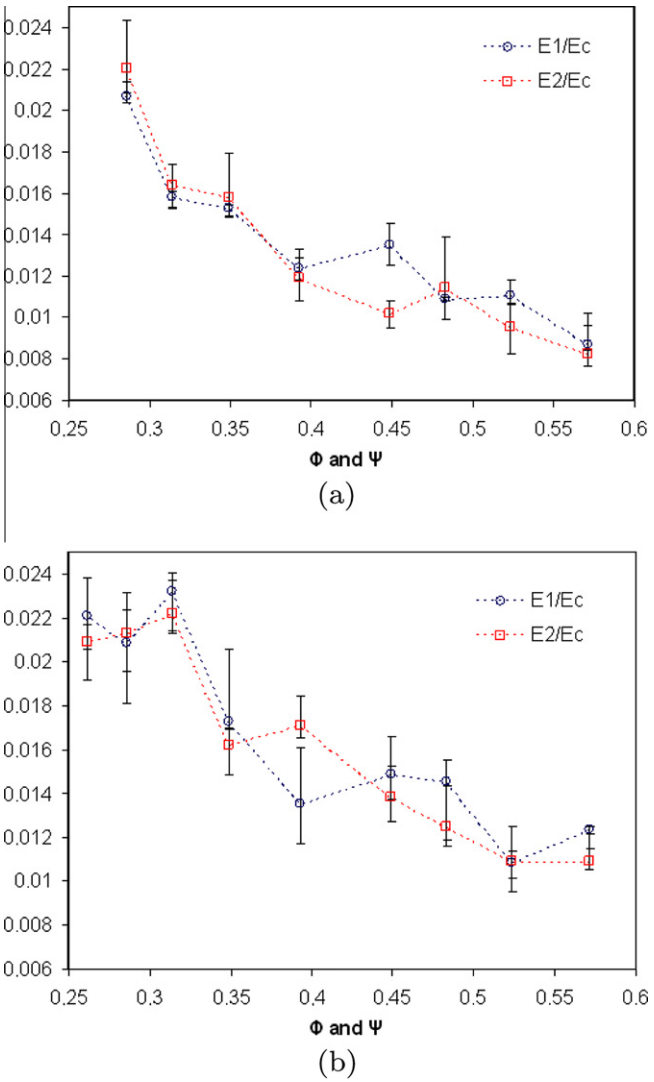

Fig. 8. The influence of the angles Φ and Ψ over the nondimensional convex honeycomb Young's modulus E_1/E_c for (a) $t = 1$ mm and (b) fixed relative density $\rho/\rho_c = 0.2$.

$E_1/E_c = C_1(\rho/\rho_c)^{2.4}$ and $E_2/E_c = C_2(\rho/\rho_c)^{2.6}$, with $C_1 = 2.43$ and $C_2 = 2.40$. The R^2 values for the two fittings are both 0.94. These formulas are valid for $0.1 \leqslant \rho/\rho_c \leqslant 0.16$. The average standard deviation for the nondimensional modulus E_1/E_c is 0.00055, while for the Young's modulus E_2/E_c is 0.009. The convex configuration described in this work when loaded along the principal direction appears to be stiffer than the regular hexagonal configuration (Gibson and Ashby, 1997), the latter having a power relation with the relative density $E/E_c = 1.5(\rho/\rho_c)^3$ (Fig. 7a). The results for the convex configurations are also consistent with the findings from (Silva et al., 1995) and (Li et al., 2005) (Fig. 7a). It is also worth noticing that Fazekas et al. have identified values of C_1 and C_2 ranging between 2.55 and 2.75 for similar intervals of large relative density ($0.05 < \rho/\rho_c \leqslant 0.3$ (Fazekas et al., 2002). The novel Voronoi-type lattices show also a complex deformation behaviour when loaded uniaxially. As an example, for a convex panel with $\Phi = \Psi = \pi/12$ (Fig. 7b), ribs associated to locations on the side of the loaded sections tend to deform predominantly by stretching. On the contrary, the ribs placed on the opposite side of the main cosine director have a bending-dominated deformation. Stretching deformations in cellular solids provide a homogenised stiffness linearly proportional to the relative density, while cellular configurations with

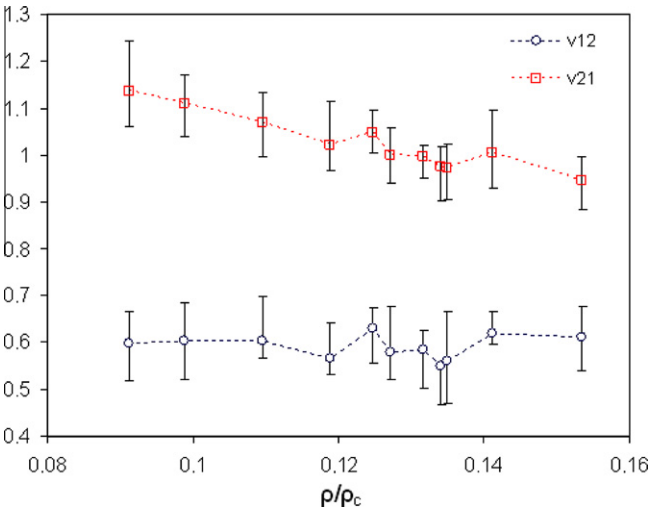

Fig. 9. Dependence of the in-plane Poisson's ratios ν_{12} and ν_{21} of the convex honeycomb versus the relative density.

the ribs dominated by bending show in-plane stiffness scaled as $(\rho/\rho_c)^3$ (Gibson and Ashby, 1997). Similarly to the structures analysed by Fazekas et al. (2002), the exponents 2.4 and 2.6 identified for the dependency of the stiffness versus the relative density are indicative of the complex deformation mechanism ongoing in the lattices. The novel Voronoi-type assembly shows an almost direct proportionality against equal pairs of angles Φ and Ψ (Fig. 8). For example, when keeping a constant relative density of 0.2 it is possible to identify the relation $E_1/E_c = -0.036\Psi + 0.031$, with $R^2 = 0.80$. An improved quality in the linear approximation arises when the thickness t of the rib is kept constant, resulting in $E_1/E_c = -0.04\Psi + 0.032$ with $R^2 = 0.92$. The nondimensional Young's modulus E_2/E_c shows a similar behaviour to the E_1/E_c one. For constant rib thickness t, there is a linear decrease against the cosine directors of the type $E_2/E_c = -0.036\Psi + 0.031$ ($R^2 = 0.80$), and $E_2/E_c = -0.04\Psi + 0.032$ ($R^2 = 0.92$) for a constant relative density $\rho/\rho_c = 0.2$ (Fig. 8), like for the E_1/E_c case. The effect of the relative size between anisotropic cells and the overall representative unit volume has also been observed in gradient cellular topologies, with stiffening effects over the uniaxial properties provided by larger cellular assemblies (Lira and Scarpa, 2010).

The Poisson's ratio v_{12} is only weakly affected by the relative density, with an average value of 0.55 (Fig. 9). The other in-plane Poisson's ratio (v_{21}) decreases slowly from an average of 1.11 at 9% of relative density to a minimum of 0.92 at 15.6 % (Fig. 9). Poisson's ratios of 1 are expected in regular hexagonal honeycombs with bending-only dominated deformation modes (Gibson and Ashby, 1997), while lower values can be expected when considering the axial stretch and transverse shear deformation for higher t/L values (Scarpa et al., 2000). Regular honeycomb configurations with different aspect ratio from 1 and varying internal cell angles do exhibit different in-plane Poisson's ratio values, not equal to 1 (Gibson and Ashby, 1997). Classical Voronoi configurations show $v_{12} = v_{21} = 0.99$ for $\rho/\rho_c = 0.1$, exhibiting therefore an isotropic in-plane behaviour (Zhu et al., 2001). For the novel type of Voronoi proposed in this work, both in-plane Poisson's ratios tend to decrease linearly with increasing cell angles Ψ and Φ, with $v_{12} = -2.508\Psi + 1.260$ and $v_{21} = -3.726\Psi + 1.9$ ($R^2 = 0.99$ and $R^2 = 0.98$ respectively – see Fig. 10). It is worth of notice the existence of negative Poisson's ratio configurations for angles $\Phi = \Psi > \pi/6$, both for v_{12} and v_{21} (Fig. 10). Higher values of the cosine director angles produce not only cells with increased anisotropy, but also cellular assemblies with reduced number of cells N_c (and therefore relative density - see Fig. 6a). Under uniaxial loading, cells with high off-axis orientations do tend to rotate, while at the same time stretching along the loading direction, therefore provide a set of non-affine deformations which are typical of negative Poisson's ratio materials (Lakes, 1991). A reduced number of cells in the representative volume element tends to amplify the non-affine deformations generated by the more off-axis orientated cells, and therefore providing a global negative Poisson's ratio effect, as observed also in other heterogeneous cellular assemblies (Horrigan et al., 2009). For lower angles Φ and Ψ, the degree of the orientation anisotropy of the cells is reduced and, at the same time, the number of cells N_c is significantly increased (see Figs. 6c and 6d). In these cases, not only the coupling between the rotation and stretching of the cells is reduced, but the effect of the most off-axis cells over the whole cellular assembly is less significant, giving to the whole convex Voronoi layout a global positive Poisson's ratio effect, with v_{21} values closer to the ones of classical Voronoi topologies (Zhu et al., 2001).

The in-plane shear modulus G_{12} follows a similar trend to the one of regular ($G_{12}/E_c = 0.375(\rho/\rho_c)^3$ (Gibson and Ashby, 1997) and Voronoi tessellations (Silva et al., 1995;Li et al., 2005) ($G_{12}/E_c = 0.354(\rho/\rho_c)^{2.89}$), albeit with a stiffening effect more evident for relative densities $\rho/\rho_c > 0.13$. It is possible to identify a relation $G_{12}/E_c = 0.39(\rho/\rho_c)^{2.9}$, with $R^2 = 0.97$ (Fig. 11). For equal cosine directors Φ and Ψ, one can observe an almost cubic relation between the normalised shear modulus and the cosine director ($G_{12}/E_c = 0.0061\Psi^{3.05}$, with $R^2 = 0.99$). Within the range of cosine directors considered, the normalised shear modulus varies between 0.05% to 1.1% (Fig. 11) (see Fig. 12).

3.2. Re-entrant configurations

Contrary to the convex configurations, the honeycombs featuring re-entrant shape cells show a linear dependence of the in-plane stiffness properties versus the relative density for $0.1 < \rho/\rho_c < 0.24$. The nondimensional Young's modulus E_1/E_c is described by a curve $E_1/E_c = 0.058(\rho/\rho_c) - 0.003$ ($R^2 = 0.92$ – Fig. 13). A similar trend (although with slightly higher stiffness) is also observed for $E_2/E_c = 0.07(\rho/\rho_c) - 0.0047$ ($R^2 = 0.92$ also in this case). The average standard deviations for E_1/E_c and E_2/E_c

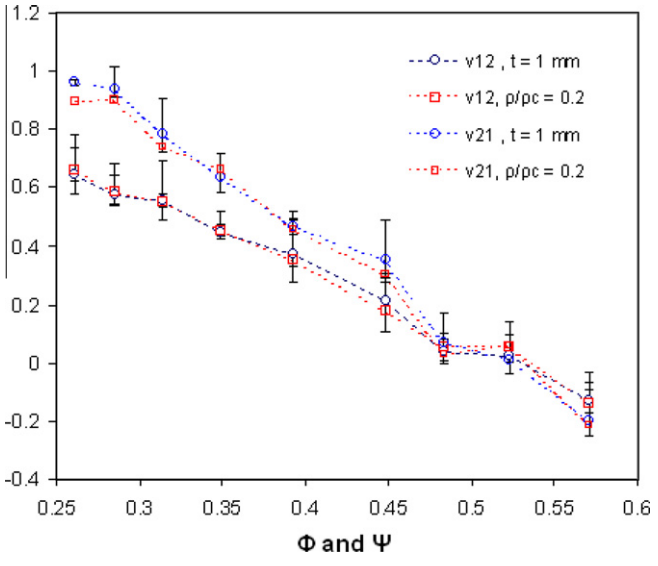

Fig. 10. Variation of the in-plane Poisson's ratios v_{12} and v_{21} of the convex honeycomb versus Φ and Ψ. Constant thickness of $t = 1$ mm and relative density of 0.2 constant.

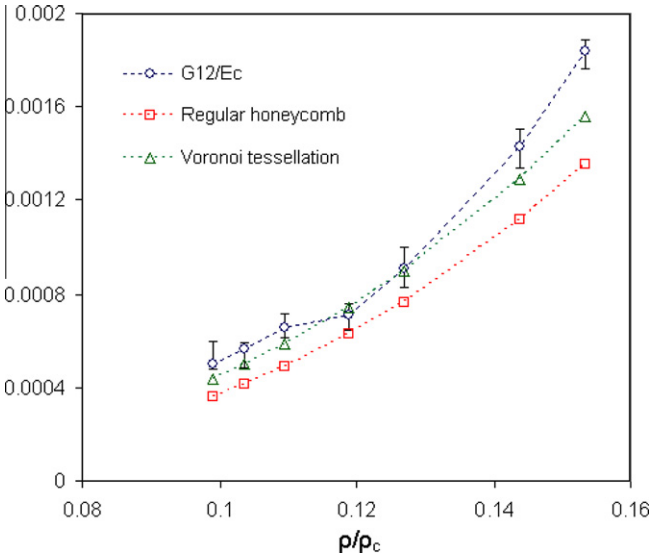

Fig. 11. Normalised shear modulus versus the relative density for the convex and regular (Voronoi) honeycomb.

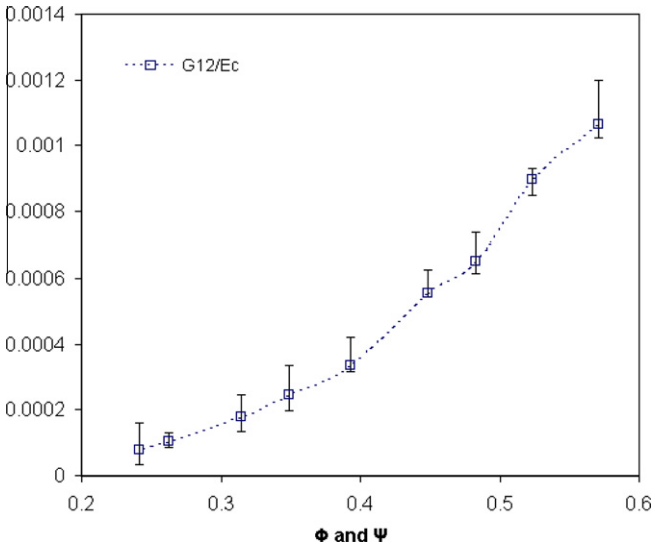

Fig. 12. Dependence of G_{12}/E_c versus the cosine directors Φ and Ψ.

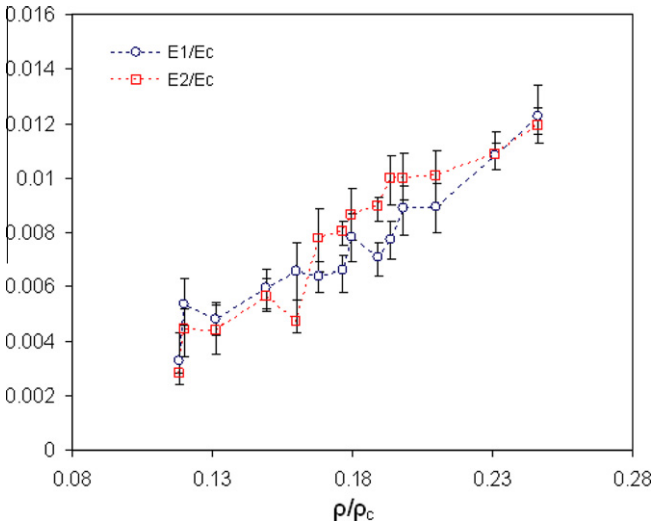

Fig. 13. Variation of the nondimensional Young's moduli E_1/E_c and E_2/E_c versus the relative density (constant thickness $t = 1$ mm) for the re-entrant Voronoi topologies.

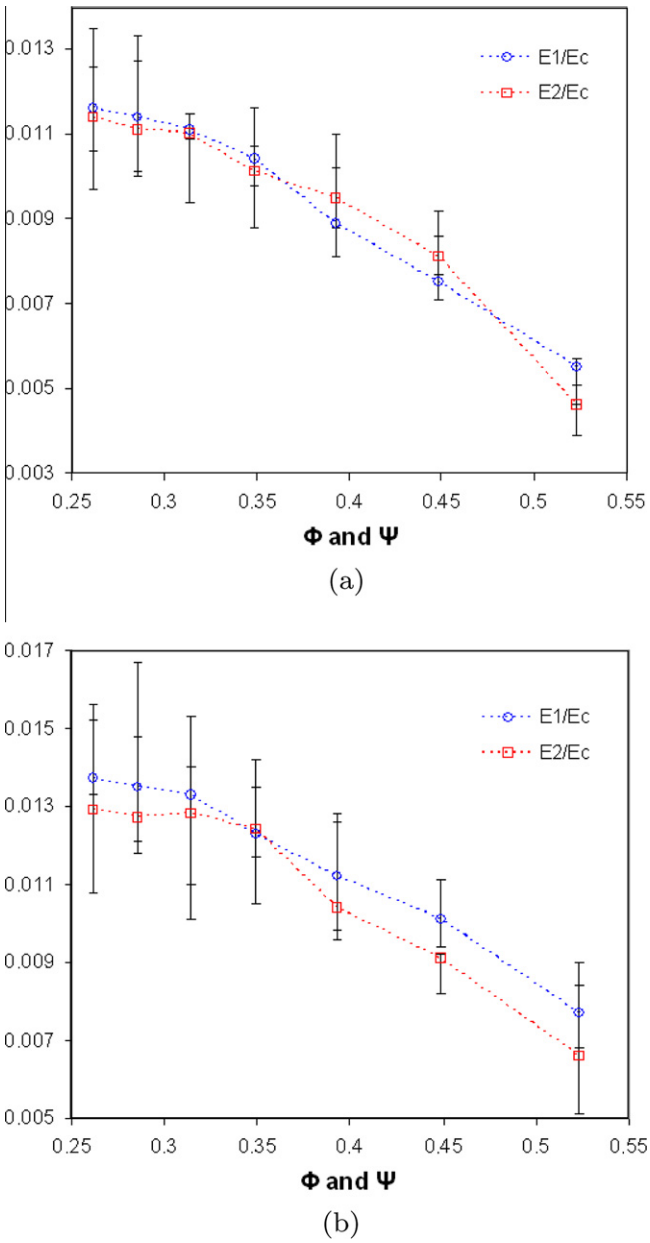

Fig. 14. The influence of the angles Φ and Ψ over the nondimensional re-entrant honeycomb Young's moduli E_1/E_c and E_2/E_c for (a) $t = 1$ mm and (b) fixed relative density $\rho/\rho_c = 0.2$.

are 0.007 for both nondimensional groups. These stiffness values are on average 2.4 times higher than the ones shown by the convex honeycomb types. These results are noteworthy, because centrosymmetric honeycomb configurations with re-entrant cells do show increased in-plane Young's moduli when compared against regular hexagonal honeycombs. Moreover, in regular re-entrant centrosymmetric cells only one in-plane Young's modulus (E_1 following the convention in Gibson and Ashby (1997) and Scarpa et al. (2000)) is increased, and only when small internal cell angles and low aspect ratios are present in the unit cell geometry (Scarpa et al., 2000). The two nondimensional Young's moduli follow also similar trends against the angles of the cosine directors, with a decrease of their modulus for increasing angles (Fig. 14a and 14b). For a constant relative density of 0.2, it is possible to identify linear regressions of the type $E_1/E_c = -0.024\Phi + 0.019$ ($R^2 = 0.93$) and $E_2/E_c = -0.025\Phi + 0.018$ ($R^2 = 0.93$), while similar behaviours do exist also when considering a constant thickness t (Fig. 14a, $E_1/E_c = -0.023\Phi + 0.02$, $R^2 = 0.98$ and $E_2/E_c = -0.025\Phi + 0.02$, $R^2 = 0.94$).

The in-plane Poisson's ratios ν_{12} and ν_{21} exhibit a different behaviour for increasing relative density. While ν_{12} shows only a marginal auxetic behaviour (average of −0.022, with average standard deviation of 0.00027), the Poisson's ratio ν_{21} assumes lower values for low relative densities, with a minimum average value of −0.67 for $\rho/\rho_c = 0.118$ (Fig. 15). This behaviour is compatible with the one observed between auxetic foams with different densities and produced following the same manufacturing route, where denser foams to tend to show Poisson's ratios with lower magnitude (Bianchi et al., 2008; Bianchi et al., 2010). However, the re-entrant Voronoi-type structure does not show a special orthotropic behaviour ($E_1\nu_{21} \neq E_2\nu_{12}$). The lowering of the Poisson's ratio ν_{21} versus increasing magnitude of the angle pair Φ and Ψ is also evident for the re-entrant cellular configurations, exhibiting on average $\nu_{21} \cong -0.87$ for $\Phi = \Psi = \pi/6$, and −0.44 for $\Phi = \Psi = \pi/10$ (Fig. 16). The Poisson's ratio ν_{12} remains marginally auxetic for the range of angles considered, with average values

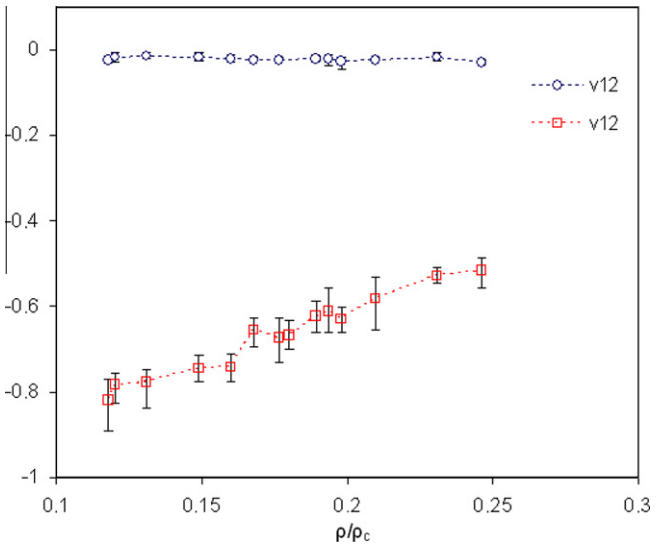

Fig. 15. Variation of v_{21} and v_{12} versus the relative density and constant thickness ($t = 1$ mm) for the re-entrant configurations.

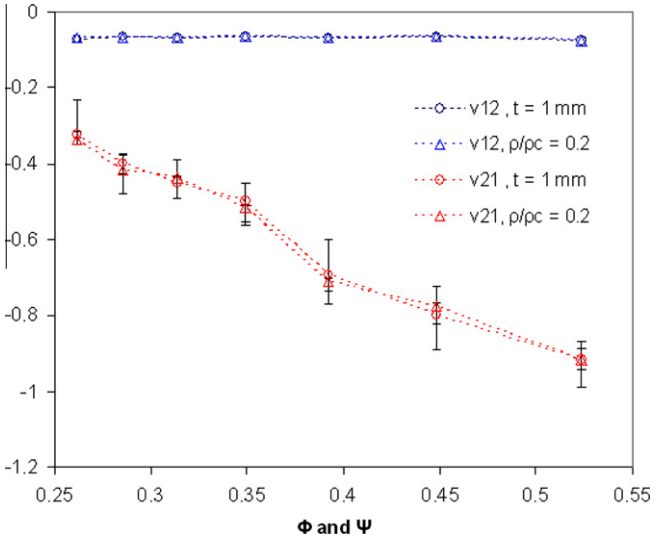

Fig. 16. Variation of the in-plane Poisson's ratios v_{12} and v_{21} of the re-entrant honeycomb versus Φ and Ψ. Constant thickness of $t = 1$ mm and $\rho/\rho_c = 0.2$ are assumed.

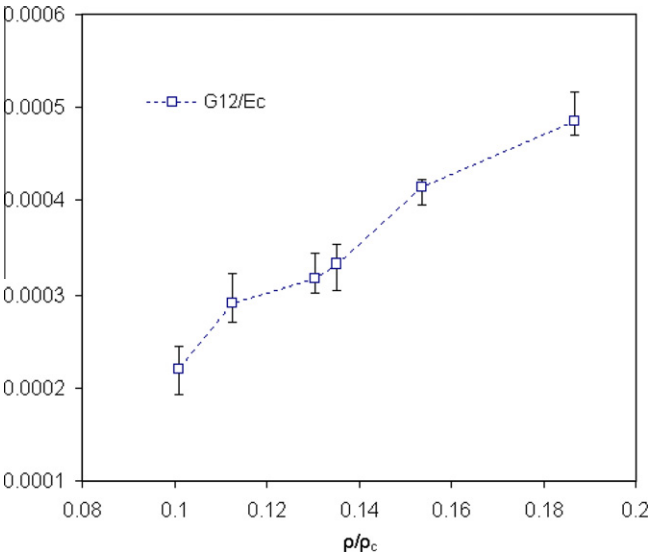

Fig. 17. Variation of the normalised shear modulus versus the relative density for the re-entrant configuration.

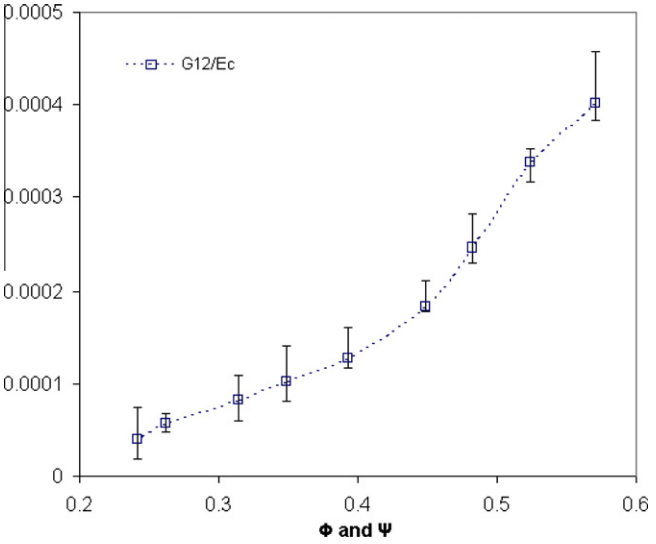

Fig. 18. Dependence of the normalised shear modulus for the re-entrant configuration versus the cosine directors.

of −0.07. It is worth noticing that the re-entrant cellular configuration remains auxetic when loaded along the two principal directions $(1, 2)$ as for the case of regular centrosymmetric re-entrant structures (Gibson and Ashby, 1982; Scarpa et al., 2000).

The normalised shear modulus G_{12}/E_c shows a similar dependency versus the relative density to the one observed for the convex configurations (Fig. 17), and a monotonic dependence towards Φ and Ψ (Fig. 18). A Least-Squares fitting lead to a linear relation of the type $G_{12}/E_c = 0.003(\rho/\rho_c)$, with $R^2 = 0.97$. The re-entrant (auxetic) configurations are significantly less stiff. For example, for $\rho/\rho_c = 0.14$ the re-entrant topology provides a normalised shear modulus 3.5 times lower than the convex configuration, but also 2.6 and 2.4 times lower than the conventional hexagonal and Voronoi tessellation respectively. A lower in-plane shear modulus G_{12} is also observed for centrosymmetric honeycombs with negative internal cell angles (Gibson and Ashby, 1997). The re-entrant configurations presented in this work appear however to be stiffer than the hexagonal chiral ones evaluated using a micropolar theory approach for small values of ρ/ρ_c (Spadoni and Ruzzene, 2012). For a relative density of 3.5%, the re-entrant Voronoi-type topology has a value of G_{12}/E_c 2.02 times higher for small chiral aspect ratios ($L/R = 0.2$). However, for hexagonal chiral configurations with very slender topology ($L/R \to 1$) the opposite is true, with the hexachiral honeycomb exhibiting a normalised shear modulus up to 78 times higher (Spadoni and Ruzzene, 2012).

4. Conclusions

The two classes of anisotropic Voronoi-type cellular structures proposed in this work provide different uniaxial stiffness and Poisson's ratio effects in the plane. The convex type has higher stiffness than a regular hexagonal and classical Voronoi configuration respectively. Moreover, the convex lattice shows a decreasing Poisson's ratio with the magnitude of the angles related to the cosine directors defining the anisotropy of the system. The in-plane shear modulus of the convex topology shows similar values to the ones

provided by regular hexagonal and Voronoi tessellations. Auxetics (i.e., negative Poisson's ratio) configurations can be achieved for angles $\Phi = \Psi > \pi/6$. The re-entrant honeycomb layouts show a lower in-plane stiffness compared to the hexagonal and classical Voronoi configurations, with equivalent nondimensional Young's moduli along the two global Cartesian loading directions, while at the same time exhibiting a global auxetic effect within the relative density range and cosine director angles considered in this work. The decrease in in-plane stiffness for the auxetic configurations is also observed for the shear modulus. The deformation mechanisms of the ribs belonging to these novel Voronoi diagrams show a combination of bending and stretching, with areas of the lattices more subjected to a deformation mechanism than the other depending on their relative position to the direction of the main cosine directors. The Voronoi-type structures described in this work may suggest ways to design porous materials and cellular configurations possessing at the same time disorder and preferential properties in the space.

References

Almgren, R., 1985. An isotropic three dimensional structure with Poisson's ratio = −1. Journal of Elasticity 15, 427–430.

Andrews, E.W., Gibson, L.J., 2001. The role of cellular structure in creep of two dimensional cellular solids. Materials Science and Engineering A 303, 120–126.

ANSYS Release 11.0 Users Manual, 2008. Swanson Inc., Canongsburg, PA.

Bezazi, A., Scarpa, F., 2007. Mechanical behaviour of conventional and negative Poisson's ratio thermoplastic polyurethane foams under compressive cyclic loading. International Journal of Fatigue 29 (5), 922–930.

Bezazi, A., Scarpa, F., 2009. Tensile fatigue of conventional and negative Poisson's ratio open cell PU foams. International Journal of Fatigue 31 (3), 488–494.

Bianchi, M., Scarpa, F., Smith, C., 2008. Stiffness and energy dissipation in polyurethane auxetic foams. Journal of Materials Science 43 (17), 5851–5860.

Bianchi, M., Scarpa, F., Smith, C., 2010. Shape memory behaviour in auxetic foams: mechanical properties. Acta Materialia 58 (3), 858–865.

Choi, J., Lakes, R., 1995. Analysis of elastic modulus of conventional foams and of re-entrant foam materials with a negative Poisson's ratio. International Journal of Mechanical Sciences 37 (1), 51–59.

Fazekas, A., Dendievel, R., Salvo, L., Brechet, Y., 2002. Effect of microstructural topology upon the stiffness and strength of 2D cellular structures. International Journal of Mechanical Sciences 44, 2047–2066.

Gibson, L.J., Ashby, M.F., 1982. The mechanics of three-dimensional cellular materials. Proceedings of the Royal Society of London. A. Mathematical and Physical Sciences 382 (1782), 43–59.

Gibson, L.J., Ashby, M.F., 1997. Cellular Solids – Structure and Properties. Cambridge Solid State Science. Cambridge University Press.

Gong, L., Kyriakides, S., Jang, W.-Y., 2005. Compressive response of open-cell foams Part I: Morphology and elastic properties. International Journal of Solids and Structures 42 (5–6), 1355–1379.

Grima, J., Gatt, R., Ravirala, N., Alderson, A., Evans, K., 2006. Negative Poisson's ratios in cellular foam materials. Materials Science and Engineering: A 423 (1–2), 214–218.

Horrigan, E., Smith, C., Scarpa, F., Gaspar, N., Javadi, A., Berger, M., Evans, K., 2009. Simulated optimisation of disordered structures with negative Poisson's ratios. Mechanics of Materials 41 (8), 919–927.

Kraynik, A.M., Reinelt, D.A., van Swol, F., 2003. Structure of random monodisperse foam. Physical Review E 67, 031403, 11 pages.

Lakes, R., 1987. Foam structures with a negative Poisson's ratio. Science 235, pp. 1038–1040.

Lakes, R., 1991. Deformation mechanisms in negative poisson's ratio materials: structural aspects. Journal of Materials Science 26, 2287–2292.

Li, K., Gao, X.L., Subhash, G., 2005. Effects of cell shape and cell wall thickness variations on the elastic properties of two dimensional cellular solids. International Journal of Solids and Structures 42, 1777–1795.

Lira, C., Scarpa, F., 2010. Transverse shear stiffness of thickness gradient honeycombs. Composites Science and Technology 70 (6), 930–936.

Lucarini, V., 2008. From symmetry breaking to Poisson point process in 2D Voronoi tessellations: the generic nature of hexagons. Journal of Statistical Physics 130, 1047–1062.

Masters, I., Evans, K., 1996. Models for the elastic deformation of honeycombs. Composite Structures 35 (4), 403–422.

McDonald, S., Ravirala, N., Withers, P., Alderson, A., 2009. In situ three-dimensional X-ray microtomography of an auxetic foam under tension. Scripta Materialia 60, pp. 232–235.

Mills, N.J., 2005. The wet Kelvin model for air flow through open-cell polyurethane foams. Journal of Materials Science 40, 5845–5851.

Oliveira, F.C., Dias, S., Vaz, M.F., Fernandes, J.C., 2006. Behaviour of open-cell cordierite foams under compression. Journal of the European Ceramic Society 26 (1–2), 179–186.

Qiang, D., Vance, F., Gunzburger, M., 1999. Centroidal Voronoi tessellations: applications and algorithms. SIAM Review 41 (4), 637–676.

Scarpa, F., Panayiotou, P., Tomlinson, G., 2000. Numerical and experimental uniaxial loading on in-plane auxetic honeycombs. The Journal of Strain Analysis for Engineering Design 35 (5), 383–388.

Scarpa, F., Burriesci, G., Smith, F.C., Chambers, B., 2003. Mechanical and electromagnetic behaviour of auxetic honeycomb structures. The Aeronautical Journal 2774, 75–183.

Schwerdtfeger, J., Schury, F., Stingl, M., Wein, F., Singer, R.F., Korner, C., 2011. Mechanical characterisation of a periodic auxetic structure produced by SEBM. Physica Status Solid (b). http://dx.doi.org/10.1002/pssb.201084211.

Silva, M.J., Hayes, W.C., Gibson, L.J., 1995. The effects of non-periodic microstructure on the elastic properties of two-dimensional cellular solids. International Journal of Mechanical Sciences 37 (11), 1161–1177.

Spadoni, A., Ruzzene, M., 2012. Elasto-static micropolar behavior of a chiral auxetic lattice. Journal of the Mechanics and Physics of Solids 60, 156–171.

Warren, W.E., Kraynik, A.M., 1997. Linear elastic behavior of a low-density Kelvin foam with open cells. Journal of Applied Mechanics 64 (4), 787–794.

Weaire, D., 2008. Kelvin's foam structure: a commentary. Philosophical Magazine Letters 88, 91–102.

Zhu, H., Knott, J., Mills, N., 1997. Analysis of the elastic properties of open–cell foams with tetrakaidecahedral cells. Journal of the Mechanics and Physics of Solids 45, 319–343.

Zhu, H.X., Hobdell, J.R., Windle, A.H., 2001. Effects of cell irregularity on the elastic properties of 2D Voronoi honeycombs. Journal of the Mechanics and Physics of Solids 49, 857–890.

Zhu, H.X., Thorpe, S.M., Windle, A.H., 2006. The effect of cell irregularity on the high strain compression of 2D Voronoi honeycombs. International Journal of Solids and Structures 43, 1061–1078.